Bioconjugation of Calcium Phosphosilicate Composite Nanoparticles for Selective Targeting of Human Breast and Pancreatic Cancers *In Vivo*

Brian M. Barth,[‡,⊥] Rahul Sharma,[†,⊥] Erhan İ. Altınoğlu,[†] Thomas T. Morgan,[†] Sriram S. Shanmugavelandy,[‡] James M. Kaiser,[‡] Christopher McGovern,[§] Gail L. Matters,[§] Jill P. Smith,[§] Mark Kester,[†] and James H. Adair[†,*]

[†]Department of Materials Science and Engineering, The Pennsylvania State University, University Park, Pennsylvania 16802, [‡]Department of Pharmacology, The Pennsylvania State Milton S. Hershey Medical Center, Hershey, Pennsylvania 17033, and [§]Department of Medicine, The Pennsylvania State Milton S. Hershey Medical Center, Hershey, Pennsylvania 17033. [⊥]The authors contributed equally to this work.

ABSTRACT The early diagnosis of cancer is the critical element in successful treatment and long-term favorable patient prognoses. The high rate of mortality is mainly attributed to the tendency for late diagnoses as symptoms may not occur until the disease has metastasized, as well as the lack of effective systemic therapies. Late diagnosis is often associated with the lack of timely sensitive imaging modalities. The promise of nanotechnology is presently limited by the inability to simultaneously seek, treat, and image cancerous lesions. This study describes the design and synthesis of fluorescent calcium phosphosilicate nanocomposite particles (CPNPs) that can be systemically targeted to breast and pancreatic cancer lesions. The CPNPs are a ~20 nm diameter composite composed of an amorphous calcium phosphate matrix doped with silicate in which a near-infrared imaging agent, indocyanine green (ICG), is embedded. In the present studies, we describe and validate CPNP bioconjugation of human holotransferrin, anti-CD71 antibody, and short gastrin peptides *via* an avidin—biotin or a novel PEG—maleimide coupling strategy. The conjugation of biotinylated human holotransferrin (diferric transferrin) and biotinylated anti-CD71 antibody (anti-transferrin receptor antibody) to avidin-conjugated CPNPs (Avidin-CPNPs) permits targeting of transferrin receptors, which are highly expressed on breast cancer cells. Similarly, the conjugation of biotinylated pentagastrin to Avidin-CPNPs and decagastrin (gastrin-10) to PEG-CPNPs *via* PEG—maleimide coupling permits targeting of gastrin receptors, which are overexpressed in pancreatic cancer lesions. These bioconjugated CPNPs have the potential to perform as a theranostic modality, simultaneously enhancing drug delivery, targeting, and imaging of breast and pancreatic cancer tumors.

KEYWORDS: bioconjugation · transferrin receptor · gastrin receptor · breast cancer · pancreatic cancer · calcium phosphate · whole animal imaging

Calcium phosphosilicate nanoparticles (CPNPs) have been engineered to be a nontoxic vehicle for the delivery of a diverse range of therapeutic and imaging agents in biological systems.[1−4] Previous studies have shown that encapsulation within CPNPs improved the lifetime and quantum properties of fluorescent dyes.[1,4] Initial *in vivo* imaging trials demonstrated that CPNPs, functionalized with polyethylene glycol (PEG) moieties, accumulated within solid tumors *via* an enhanced permeation retention (EPR) effect.[2] While EPR serves as an effective passive targeting strategy, particular interest lies in the ability to actively target cancerous cells to deliver anti-neoplastic agents, thereby decreasing effective dosage and limiting off-target toxicity.

CPNPs are nontoxic, colloidally stable, nanoscale vehicles that deliver chemotherapeutics and imaging agents. Two exciting aspects of CPNPs as drug delivery vehicles include enterohepatic biliary excretion that minimizes hepatic toxicity and pH-triggered release of active agents. At pH 7.4, the CPNPs are sparingly soluble, but the CPNPs dissolve in the late stage endolysosomes at pH 4 to 5.[1,4] The pH response of CPNPs produces two effects. First, it permits a decrease in the effective dose of potentially toxic chemotherapeutic drugs required for optimal therapeutic benefit by increasing the efficiency of drug delivery into cancer cells.[3] Second, sequestering the drug in the CPNPs decreases the effective concentration of free drug present in the extracellular fluid where the pH is maintained at approximately pH 7.4 by physiological buffers. This compartmentalization feature for drug delivery produces advantages since acute systemic toxicity to normal cells is limited. Moreover, off-site cytotoxicity may be further ameliorated with target- and tissue-specific CPNPs.

Scientific investigations have identified cancer cell specific markers with unique phenotypes that can be exploited to target tumors. Of particular interest is the prevalence of transferrin receptors (CD71) on

*Address correspondence to jha3@ems.psu.edu.

Received for review September 25, 2009 and accepted February 11, 2010.

Published online February 24, 2010. 10.1021/nn901297q

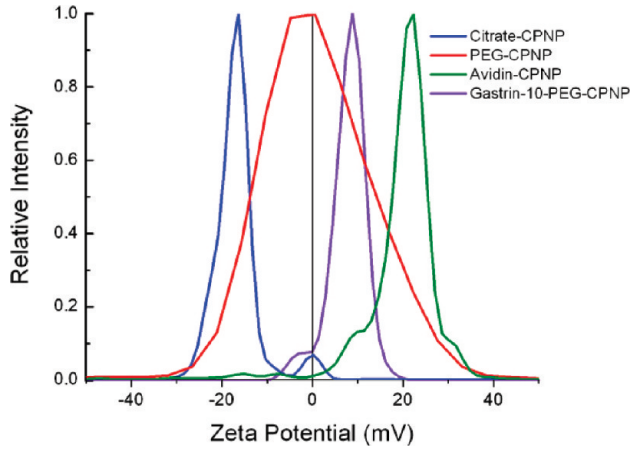

Figure 1. Zeta potential distributions for Citrate-CPNPs, Avidin-CPNPs, PEG-CPNPs, and Gastrin-10-PEG-CPNPs. The Citrate-CPNPs (blue line) displayed a mean ζ potential of −16 ± 1.3 mV, whereas PEGylation shifted the mean ζ potential to +3.0 ± 2.0 mV (red), gastrin-10 conjugation further shifted the mean ζ potential to +6 ± 3.2 mV (violet), and the Avidin-CPNPs (green line) had a mean ζ potential value of +29 ± 8.7 mV. All ζ potential distributions represent the average of three independent experiments.

cancerous cells, including breast cancer.[5−9] The transferrin receptor is responsible for transporting iron, *via* interaction with transferrin, into cells as demanded by metabolic need.[5,6] Accordingly, transferrin receptors are found predominately on proliferating cells with elevated metabolic levels, including many cancerous cells, as well as brain capillary endothelial cells and hematopoietic cells.[10,11] In a manner similar to CD71, gastrin receptors have a predominate prevalence within certain tissues, specifically the gastrointestinal and central nervous systems.[12−14] The hormone gastrin binds to a family of G-protein-coupled receptors, also known as the cholecystokinin-2 (CCK_2 or CCK-B) receptor family,[14,15] and is typically known as a key mediator of stomach acidity[16] and growth of the gastrointestinal tract.[17] Intriguingly, CCK_2 receptor expression is often increased in many cases of gastrointestinal cancer,[13,18] including pancreatic cancer,[19] and, in particular, an increase in the expression of a specific splice variant (CCK_{2i4sv} or CCK-C) of the receptor.[20]

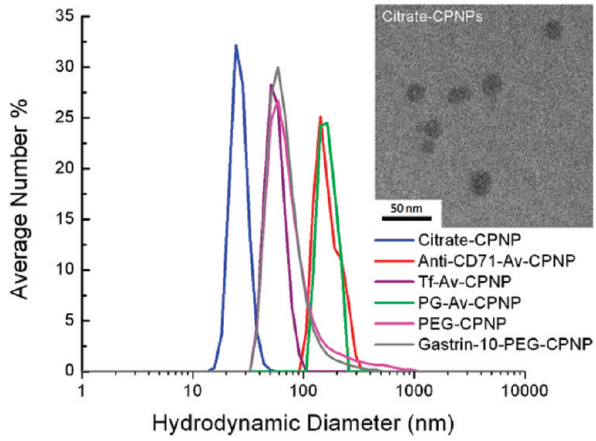

Figure 2. Dynamic light scattering determinations for Citrate-CPNP, Anti-CD71-Avidin-CPNPs (Anti-CD71-Av-CPNP), Human Holotransferrin-Avidin-CPNPs (Tf-Av-CPNP), Pentagastrin-Avidin-CPNPs (PG-Av-CPNP), maleimidePEG-CPNPs (PEG-CPNP), and Gastrin-10-maleimidePEG-CPNPs (Gastrin-10-PEG-CPNP). All dynamic light scattering determinations are the mean of three independent experiments. Inset shows a typical TEM micrograph of Citrate-CPNPs.

Despite many new advances in the arsenal of antineoplastic agents, drug-resistant, highly metastatic cancers continue to ravage patients.[21] As examples, breast cancer is still the second leading cause of death in American women with an estimated 192 370 cases diagnosed in 2009. In this year alone, about 40 610 women will die from breast cancer in the United States. Pancreatic cancer is the fourth leading cause of cancer-related deaths in the United States. Approximately 42 470 Americans were diagnosed with pancreatic cancer in the past year, and nearly 100% will succumb to this disease.[21] It is clear that new modalities are needed that have the capabilities to improve both diagnosis and treatment of cancers. The term theranostic has been coined to describe modalities that can simultaneously diagnose and treat. Our studies describe the *in vivo* validation of a nano "solution" that can actively target and image breast and pancreatic cancer lesions.

RESULTS AND DISCUSSION

Physical Characterization of CPNPs. Citrate-functionalized CPNPs were utilized as a platform for functionalization, which allowed the characterization of bioconjugation *via* ζ potential analysis (Figure 1). Figure 1 shows the ζ potential distribution of Citrate-CPNPs prior to bioconjugation (blue line) and the ζ potential distributions of the Avidin-CPNP complex (green), maleimide-terminated polyethylene glycol (PEG)-coated CPNPs (red), and CPNPs conjugated with gastrin-10 *via* a maleimide−PEG coupling (violet). Prior to bioconjugation, the Citrate-CPNPs display a negative mean ζ potential value of −16 ± 1.3 mV, which is consistent with previous reports.[1] However, after bioconjugation, the Avidin-CPNPs displayed a relatively high positive mean ζ potential value of +29 ± 8.7 mV. The isoelectric point for avidin is pH 10. Thus, the shift from a negative ζ potential to a positive ζ potential distribution is strong evidence of avidin bioconjugation on the surface of CPNPs. Also, Figure 1 shows the shift in mean ζ potential to +3.0 ± 2.0 mV when coated with the PEG and then a further shift to +6 ± 3.2 mV when conjugated to gastrin-10.

Further characterization was used to confirm the presence and bioactivity of the bioconjugated Avidin-CPNPs for biotin. A 2,6-ANS titration was used to confirm both the presence of avidin and its associated bioactivity. An analysis of the particle size distributions of the nanoparticles *via* dynamic light scattering (DLS) revealed that all of the various bioconjugated CPNPs had a larger mean hydrodynamic diameter than the nonbioconjugated Citrate-CPNPs (Figure 2). Transmission electron microscopy (TEM) analysis indicated that the inor-

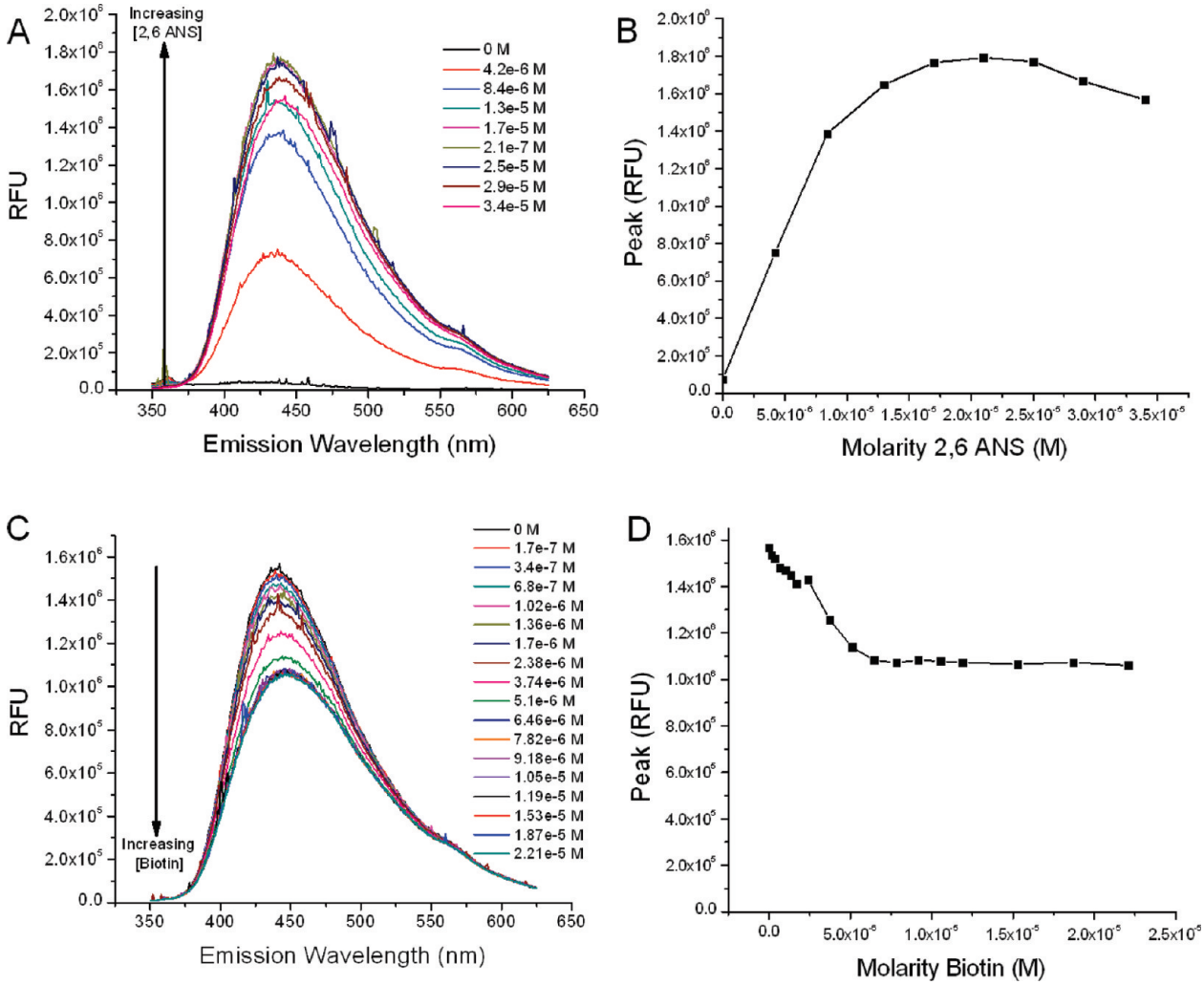

Figure 3. Displacement of 2,6-ANS was utilized to evaluate the coupling of biotin to Avidin-CPNPs. (A) Fluorescence intensities for the first step of the 2,6-ANS assay. The addition of 2,6-ANS to the Avidin-CPNP complex results in a 6-fold increase in fluorescence as the fluorescent probe binds to the biotin binding site on avidin. The 2,6-ANS was added at increasing concentrations to Avidin-CPNPs, and increased fluorescence, indicative of 2,6-ANS bound to avidin, was quantitatively determined. (B) Peak height of fluorescence shown in panel A as a function of 2,6-ANS molarity. (C) Fluorescence intensities for the second step of the 2,6-ANS assay. The addition of biotin to the 2,6-ANS-Avidin-CPNP complex results in a decrease in fluorescence as biotin displaces the fluorescent probe from the biotin-binding site on avidin. Biotin was added at increasing concentrations to the 2,6-ANS-Avidin-CPNP complex, and a decrease in fluorescence, indicative of biotin displacing 2,6-ANS, was quantitatively determined. (D) Peak height of fluorescence shown in panel C as a function of biotin molarity. All determinations are representative of three independent experiments.

ganic particle size was in the range from 10 to 30 nm for all of the CPNPs (inset Figure 2). The smaller size *via* TEM relative to DLS analyses is consistent with the ability to determine the solid material diameter *via* the TEM technique in contrast to DLS, which gives the hydrodynamic size distribution in colloidal suspension of solid particle, organic layers, and surrounding liquid.

Previous studies have demonstrated that a 2,6-ANS assay can be utilized to evaluate the biotin-binding functionality of avidin.[22] The 2,6-ANS fluorescent probe binds to avidin, an event that can be measured using fluorescence spectroscopy. Without avidin present, the 2,6-ANS fluorescent probe displays low fluorescence intensity. In the presence of avidin, the binding of 2,6-ANS to the biotin-binding site on avidin produces an increase in fluorescence intensity. The 2,6-ANS was therefore added in increasing concentrations to the Avidin-CPNPs, and a concentration-dependent increase in 2,6-ANS fluorescence emission was noted (Figure 3A,B). The titration of 2,6-ANS showed an increase in fluorescence up to 1.79×10^6 RFU after the addition of 34 μM 2,6-ANS. Beyond this point of maximum fluorescence intensity, the 2,6-ANS self-quenched, at which point biotin was added to displace the 2,6-ANS. Biotin has a greater affinity for the biotin-binding site on avidin than does the 2,6-ANS fluorescent probe. Therefore, biotin additions to the 2,6-ANS-Avidin-CPNP complex displaces the 2,6-ANS from the biotin-binding site on avidin. Since the 2,6-ANS fluorescent probe displays minimal fluorescence when it is not bound to avidin, this displacement produces a decrease in fluorescence (Figure 3C,D) to a plateau of 1.08×10^6 RFU after the addition of 1.90 nM biotin. The plateau is present in Figure 3D because of the intrinsic fluorescence of 2,6-ANS.

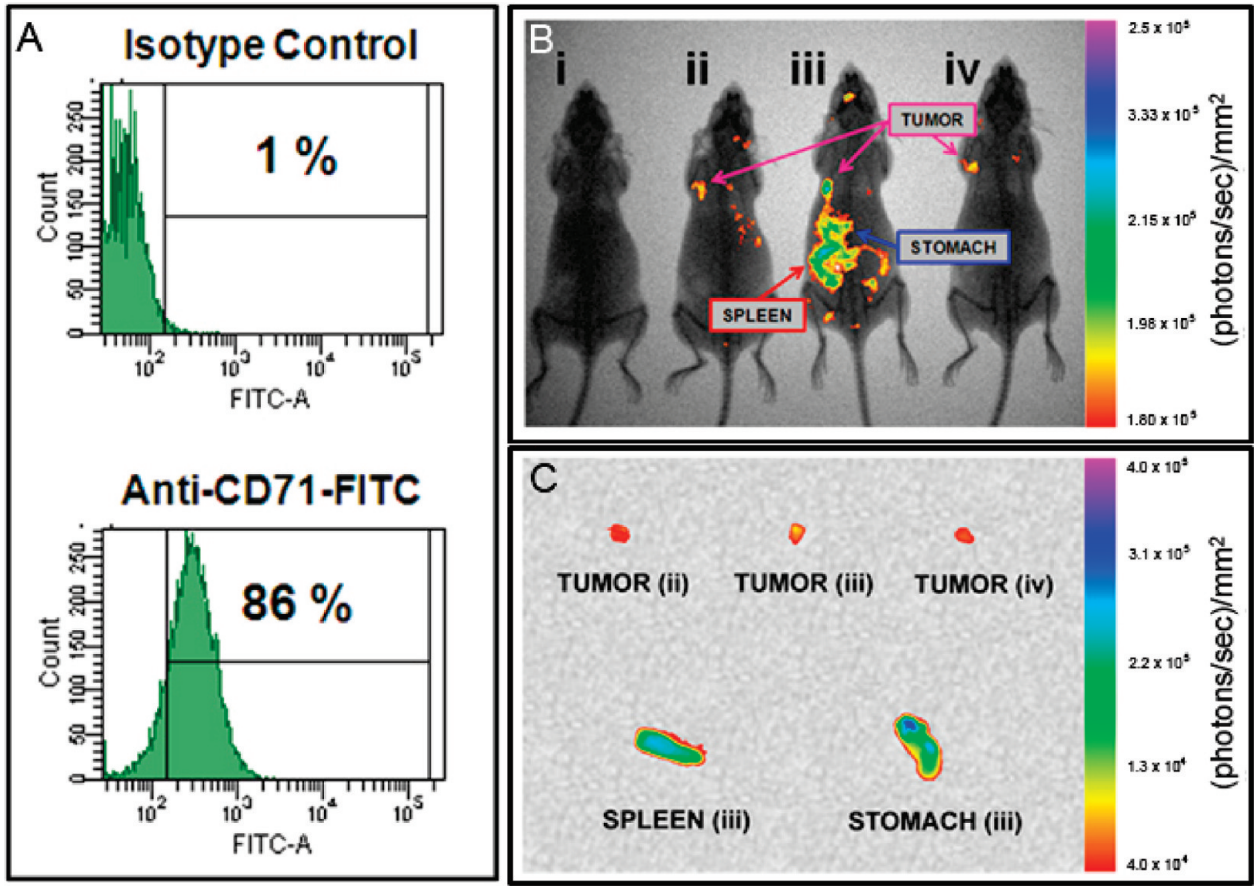

Figure 4. Targeting transferrin receptors in an *in vivo* subcutaneous tumor model of breast cancer. (A) Human MDA-MB-231 metastatic breast cancer cells were analyzed *via* flow cytometry for the presence of the transferrin receptor (CD71). (B) MDA-MB-231 cells were xenografted subcutaneously into athymic nude mice. One week following engraftment, ICG-loaded CPNPs were administered systemically *via* tail vein injection, and near-infrared images were taken 96 h post-injection. From left to right, mice received (i) free ICG, (ii) ICG-loaded PEG-CPNPs, (iii) ICG-loaded Anti-CD71-Avidin-CPNPs, or (iv) ICG-loaded Human Holotransferrin-Avidin-CPNPs. (C) Excised tumors (mice ii, iii, and iv from panel B) and spleen and stomach (mouse ii). All images are representative of four independent experiments.

This result demonstrates the successful coupling of biotin to the Avidin-CPNPs. The 2,6-ANS fluorescence emission did not decrease completely as some 2,6-ANS remains bound to the Avidin-CPNPs. While the affinity of avidin for biotin is high, residual reactants and ionic conditions can influence this affinity as it has been established that water participates in displacing biotin from the binding pocket of avidin or similar proteins.[23,24] Nonetheless, this analysis has successfully demonstrated that the Avidin-CPNPs are biofunctional, through binding of 2,6-ANS as well as its displacement by biotin.

Evaluation of Breast-Cancer-Targeted CPNPs *In Vivo*. Transferrin receptors are expressed on cells with increased metabolic demand, including several cancerous cells. The presence of the transferrin receptor (CD71) on the surface of human MDA-MB-231 cells was determined *via* flow cytometry and was found to be prevalent on nearly all cells analyzed (Figure 4A). The presence of CD71 on most MDA-MB-231 cells indicated that it would be an ideal surface target, exploited by coupling specific antibodies, or the ligand holotransferrin, to our Avidin-CPNPs. It has been previously shown that the untargeted PEG-CPNPs passively accumulate in breast cancer tumors *via* the EPR effect.[2] This finding was successfully repeated within this trial as a positive control (Figure 4B). Intriguingly, tumors from mice receiving Anti-CD71-Avidin-CPNPs, and not Human Holotransferrin-Avidin-CPNPs or untargeted PEG-CPNPs, were effectively targeted as evidenced by prominent illumination 96 h following tail vein injection of CPNPs (Figure 4B). It has been reported, and is likely in this circumstance, that the transferrin receptors are saturated with transferrin[25] and therefore are unable to bind the Human Holotransferrin-Avidin-CPNPs. This is also supported by the success of the Anti-CD71-Avidin-CPNPs, which recognize an epitope separate from the ligand-binding site on the transferrin receptor. Importantly, the Anti-CD71-Avidin-CPNPs were more effective at targeting the tumors than the passively accumulating PEG-CPNPs based on the relative fluorescence intensity. However, and not surprisingly, the effective targeting was not limited to the tumors, but also to the spleen, which is rich in a diversity of hematopoietic cells (Figure 4C). It was also observed that there was some off-target staining of the stomach (Fig-

ure 4C), possibly due to avidin interaction with biotin ingested as part of the mouse's diet or due to the presence of transferrin receptors on these tissues. Previously, clearance of PEG-CPNPs was reported to occur *via* hepatobiliary clearance evidenced by predominant staining of the liver within minutes following tail vein injection.[2] In the current study, hepatobiliary clearance was validated 24 h post-tail vein injection of PEG-CPNPs and showed the progression of signal from the liver and through the intestine as fecal matter (Figure 5). Overall, these findings showed that the transferrin receptor-targeted CPNPs were effective and selective in an *in vivo* model of breast cancer.

Evaluation of BxPC-3 Pancreatic Cell Targeting by Gastrin-Receptor-Targeted CPNPs. Increased surface expression of gastrin receptors on pancreatic tumors, and cell lines, was targeted by CPNPs coupled *via* a PEG linker to a short gastrin peptide (Gastrin-10-PEG-CPNPs). BxPC-3 human pancreatic cancer cells were treated with Gastrin-10-PEG-CPNPs or untargeted PEG-CPNPs for 5 or 60 min, followed by a replacement of media for 55 min or no change, respectively. Cells were fixed and visualized using a fluorescence microscope set up to analyze a broad range of fluorescence simultaneously. Only BxPC-3 cells exposed for 60 min to Gastrin-10-PEG-CPNPs, and no media exchange, displayed fluorescent staining (Figure 6A). Intriguingly, the observed fluorescence was green and blue, indicative of the pH-dependent degradation of CPNPs as they internalize to the endosomal−lysosomal pathway and release the encapsulated dye (fluorescein). Fluorescein displays a complex pH-dependent equilibrium and emission from its two fluorescent ionic forms, the monoanion and dianion.[26,27] In higher pH environments, such as that in the CPNPs and physiological solutions, the significant emission wavelength is from the dianion (peak excitation 495 nm, green). As pH drops below 6.5, the molecule is protonated into its monoanionic form which is excited in the blue (450 nm). Thus, emission signals from the fluorescein-encapsulating CPNPs shift from green toward blue as they experience the pH drop characteristic of the endosomal−lysosomal pathway into the cells, resulting in the dissolution of the particles and release of the fluorophore into the lower pH environment of late-stage endosomes.

Alternatively, BxPC-3 cells were exposed, fixed, and analyzed *via* flow cytometry (Figure 6B). This further showed that Gastrin-10-PEG-CPNPs (60 min exposure) targeted BxPC-3 cells while untargeted PEG-CPNPs did not.

Evaluation of Pancreatic-Cancer-Targeted CPNPs *In Vivo*. It was found that the untargeted PEG-CPNPs effectively accumulated 24 h post-tail vein injection within small BxPC-3 tumors in the pancreas (Figure 7A), and these whole animal images were confirmed by excision of the pancreas (Figure 7B). The Pentagastrin-Avidin-CPNPs, using the avidin−biotin coupling approach,

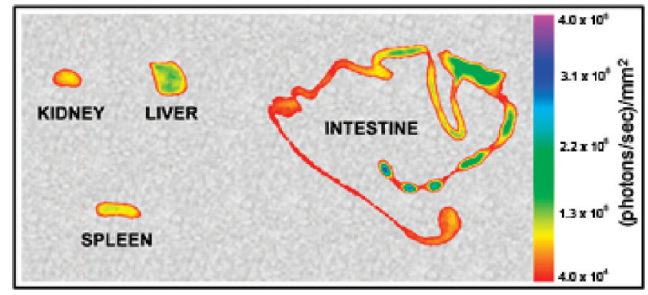

Figure 5. ICG-loaded PEG-CPNP clearance *via* hepatobiliary secretion. Twenty-four hours post-tail vein injection, the kidney, liver, spleen, and intestine were excised and imaged. Increased signal toward end of the intestine as indicated by fecal pellets within the intestine. All images are representative of three independent experiments.

also targeted the pancreatic tumors (Figure 7). However, the Gastrin-10-PEG-CPNPs proved to be much more successful at targeting the pancreatic tumors (Fig-

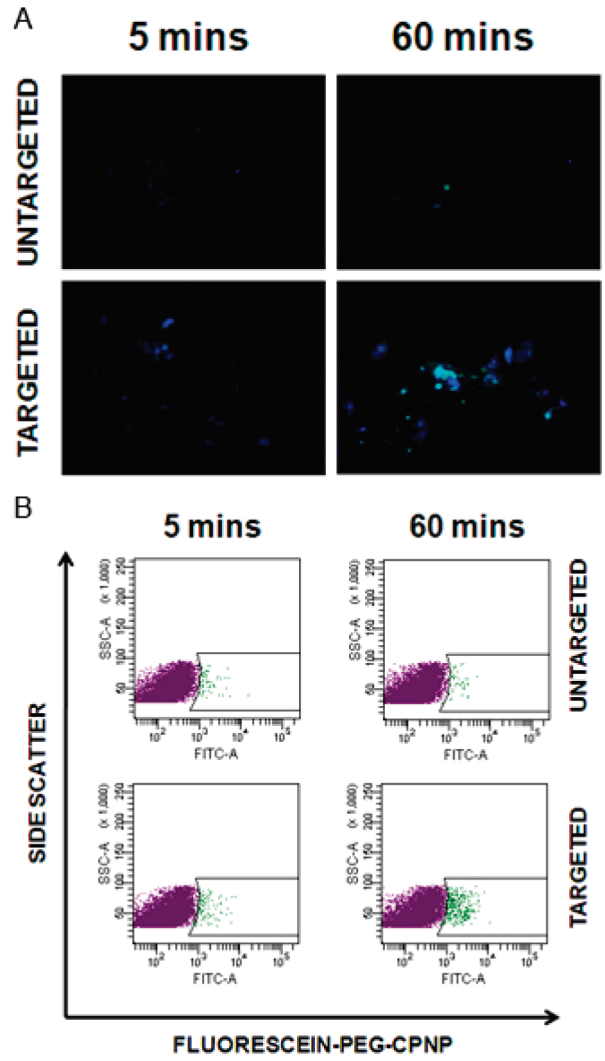

Figure 6. Gastrin-receptor-targeted CPNPs effectively targeted human BxPC-3 pancreatic cancer cells. BxPC-3 cells were exposed to fluorescein-loaded untargeted PEG-CPNPs, or Gastrin-10-PEG-CPNPs, for 5 min followed by exchange to fresh media for 55 min, or exposure for 60 min. (A) Cells were fixed and visualized by microscopy. (B) Cells were fixed and analyzed by flow cytometry with graphs representing 10 000 collected events per sample.

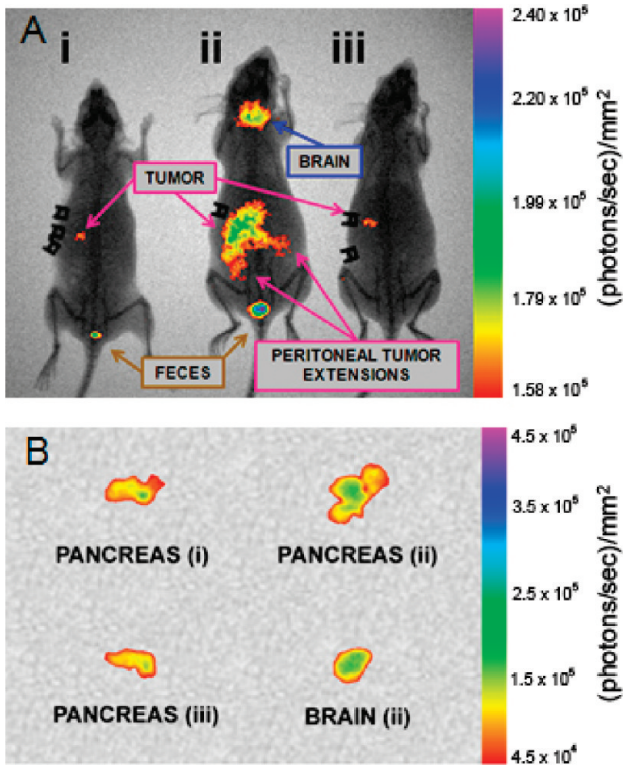

Figure 7. Targeting gastrin receptors in an *in vivo* orthotopic tumor model of pancreatic cancer. Human BxPC-3 pancreatic cancer cells were xenografted orthotopically into athymic nude mice. (A) One week following engraftment, ICG-loaded CPNPs were administered systemically *via* tail vein injection, and near-infrared images were taken 24 h post-injection. From left to right, mice received (i) ICG-loaded PEG-CPNPs, (ii) ICG-loaded Gastrin-10-PEG-CPNPs, or (iii) ICG-loaded Pentagastrin-Avidin-CPNPs. (B) Excised, tumor-bearing, pancreases from each mouse and excised brain (mouse ii). All images are representative of at least four independent experiments.

ure 7A), including peritoneal extensions of the primary tumor, as well as the brain, which is also rich in gastrin receptors.[14] We confirmed targeting of the Gastrin-10-PEG-CPNPs to the brain by excising and imaging the brain during necropsy (Figure 7B). An advantage of the later targeting approach is the covalent attachment, eliminating the possibility of nonspecific avidin interactions *in vivo*, as well as the PEG, which permits improved systemic retention and decreased immune reactivity.[2] It is also possible that the presence of avidin on the CPNPs does not permit crossing of the blood−brain barrier, whereas the PEG−maleimide bioconjugation for gastrin-10 may permit penetration of the brain−brain barrier. It is noteworthy that the untargeted PEG-CPNPs did not display any significant brain accumulation in this study. A recent study comparing interleukin-13-targeted nanoliposomes to untargeted nanoliposomes in a cranial model of glioblastoma showed that only targeted nanoliposomes moved significantly across the blood−brain barrier.[28] The current study, although using a different target and different nanoparticles (gastrin-receptor-targeted CPNPs), corroborates the other group's finding that targeted nanoparticles can cross the blood−brain barrier. Importantly, the CPNPs are biocompatible, and it has been previously shown that they exhibited no specific detrimental effects toward neurons.[3] This finding was reiterated in the current study, as no mice receiving any CPNPs showed signs of neurological deficits. Therefore, this portion of the study demonstrated that the CPNPs can be effectively targeted to gastrin receptors *in vivo* in a model of pancreatic cancer and further showed the potential for targeting across the blood−brain barrier.

CONCLUSIONS

The ability to target nanodelivery systems to specific tissues is important in the development of improved therapeutics for diseases such as cancer. In many studies and clinical circumstances, the efficacies of treatments are limited or the off-target effects are dramatic. Nanoscale therapeutics help to minimize these problems by concentrating smaller doses of therapeutic agents, yet are still limited if not targeted. Recent research has shown that molecular-specific therapeutics or targeted therapeutic delivery systems are highly efficacious and may even help to overcome complicating circumstances such as multidrug resistance.[11] Often, these studies are restricted to *in vitro* models. However, the true test for active targeting requires *in vivo* models, in which the delivery modality is administered systemically with the nanodelivery system allowed to freely circulate to localize in the desired tissue to establish efficacy of the targeting strategy and delivery system. The present study demonstrates effective systemic targeting in both a subcutaneous and an orthotopic *in vivo* model using the CPNP nanodelivery system.

The CPNPs in this study were engineered specifically as nontoxic biocompatible nanoscale delivery vehicles. It has been previously shown that a variety of molecules, including dyes that could be used in tumor detection, or hydrophobic antineoplastic agents, such as ceramide, could be encapsulated.[1−3] Until now, the CPNPs have relied on passive accumulation *via* the EPR effect for solid tumor detection. This study demonstrates that surface-targeting strategies can be successfully attached to the CPNPs, *via* two distinct coupling methods, and these bioconjugated CPNPs can effectively target select tissues *via* surface feature targeting (Figure 8). Specifically, breast cancer tumors were targeted *in vivo* by targeting transferrin receptors, and orthotopic pancreatic cancer tumors were targeted *in vivo* by targeting gastrin receptors. Additionally, our experiments confirmed that the untargeted PEG-CPNPs could accumulate moderately yet could be effectively imaged within small orthotopic pancreatic tumors, extending the diagnostic imaging capability and therapeutic delivery capabilities to one of the more evasive cancers. This study also showed that gastrin-receptor-targeted CPNPs could cross the blood−brain barrier, which may expand the utility of the CPNPs to therapeutics targeted to glioblastoma or even to neurodegenerative or psychiatric disorders.

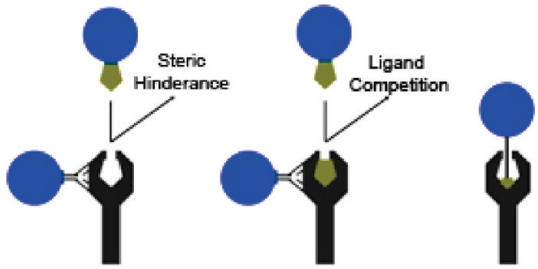

Figure 8. Receptor, or surface feature, targeting strategies and pitfalls. CPNPs were designed to target transferrin receptors (CD71) or gastrin receptors *via* antibody or ligand coupling *via* noncovalent (avidin−biotin interactions) and covalent (PEG linker) coupling strategies. Receptor-targeted CPNPs utilizing coupled antibodies may interact *via* epitopes separate from ligand-binding sites. Ligand-coupled CPNPs may interact with the receptor; however, interference can occur in the form of steric hindrance (avidin or particle interferes with interaction) or ligand competition with the natural ligand.

Even though targeted nanotechnology can be used to target specific receptors or ligands on cancer cells, there may still be obstacles, as these receptors may be expressed on other tissues. As a case in point to alleviate this shortcoming, CPNPs can potentially be "loaded" with selective gene therapies or agents to become cancer-specific. For example, although gastrin receptors are present in both malignant and some normal tissues, only the pancreatic cancer cells produce endogenous gastrin.[29] The acid-secreting parietal cells of the stomach, imaged in the current investigation with ICG-loaded, Gastrin-10-PEG-CPNPs (covalently coupled), or ICG-loaded, Pentagastrin-Avidin-CPNPs, do not produce endogenous gastrin. The only nonmalignant cells that produce gastrin in adults are the G-cells of the stomach antrum, and the G-cells do not possess gastrin receptors.[30,31] Previous studies have shown that down regulation of endogenous gastrin expression using RNA interference techniques significantly inhibits growth of pancreatic cancer tumors and metastases.[32,33] One problem with using gene therapy in animals and in humans has been in finding delivery systems that would protect the siRNA from degradation in the peripheral circulation. Since siRNA molecules are readily degraded by nucleases in the peripheral blood and tissues, mechanisms for delivery have been an active area of recent investigation. Viral vectors, especially the adeno-associated viruses (AAVs) and the adenoviruses, have been under investigation; however, hepatotoxicity and immunogenicity have been reported.[34] The use of a tissue-specific and cancer-selective vehicle such as siRNA-loaded CPNPs coupled for receptor targeting would be ideal as cancer therapeutics.

This study showed the successful bioconjugation of surface-targeting strategies to the CPNPs, demonstrating effectiveness, selectivity, and utility in two separate *in vivo* models. This study will allow the further development of the CPNPs to target a diversity of disorders, including several poor prognosis cancers and possibly even nonsolid tumors such as leukemia.

MATERIALS AND METHODS

Preparation of Nanoparticles. CPNPs were prepared by the microemulsion technique and van der Waals HPLC that have been previously described.[1−4] Cyclohexane (C_6H_{12}, BHD Chemical Co.), Igepal CO-520 ($C_{13}H_{20}O(C_2H_4O)_{n=5}$, Rhodia Chemical Co.), and deionized H_2O were used to prepare the microemulsions. Calcium chloride ($CaCl_2 \cdot 2H_2O$, Sigma-Aldrich Co.), disodium hydrogen phosphate (Na_2HPO_4, Sigma Aldrich Co.), and sodium metasilicate (Na_2SiO_3, Sigma-Aldrich Co.) were used as particle precursors. Disodium hydrogen citrate dihydrate ($HOC(COOH)(CH_2COONa)_2 \cdot 2H_2O$, Sigma-Aldrich Co.) was used as the dispersant. Indocyanine green (ICG) (TCI America Co.) was used as the near-infrared fluorophore in the CPNPs for the animal trials, while fluorescein sodium salt (Sigma-Aldrich Co.) was the visible fluorophore encapsulated for flow cell and *in vitro* experiments. Neat ethanol was purchased from VWR International. All other chemicals were obtained from Sigma-Aldrich Co., unless otherwise noted.

Two separate microemulsions (1 and 2) were formed with a cyclohexane/Igepal CO-520/water system. The molar ratio of water to surfactant was 4. Then, 650 μL of 1×10^{-2} M $CaCl_2$ in CO_2-free deionized H_2O was added to 14 mL of a 29 vol % solution of Igepal CO-520 in cyclohexane to form Microemulsion 1. Similarly, 65 μL of 6×10^{-2} M disodium hydrogen phosphate (Na_2HPO_4) with 65 μL of 8.2×10^{-3} M sodium metasilicate (Na_2SiO_3) in CO_2-free deionized H_2O (pH 7.4) was added to 14 mL of a 29 vol % solution of Igepal CO-520 in cyclohexane to form Microemulsion 2. A 520 μL aliquot of 0.01 M fluorophore in CO_2-free deionized H_2O was added into Microemulsion 2 so that the final H_2O volume matched that in Microemulsion 1 (650 μL), hence retaining the water to surfactant ratio in each. The individual microemulsions were allowed to equilibrate for 1 h before 1 and 2 were mixed to form Microemulsion 3. Microemulsion 3 was allowed to undergo micellar exchange for 2 min, during which time doped CPNPs precipitated in the micelles. A 225 μL aliquot of 1×10^{-3} M sodium citrate was added to Microemulsion 3 and allowed to react for 15 min. After adding the dispersant, the reverse micelles were dissolved with 50 mL of ethanol adjusted with 1 M KOH before laundering *via* the van der Waals HPLC.[1−4]

The unwashed CPNP suspension was loaded onto a silica HPLC (high-performance liquid chromatography) column after the micelles had been dissolved with ethanol; the free organic was laundered with ethanol adjusted with 1 M KOH as the eluent; finally, the particles were eluted using 70:30 ethanol/water by volume. During the washing step, the dye content was monitored at an absorption of 785 or 495 nm for ICG or fluorescein, respectively. The ethanol washing was continued until the detector reached baseline, indicating removal of the excess dye. The first major peak was collected. The precursor and HPLC solutions were prepared with CO_2-free deionized H_2O to avoid carbonate contamination in the CPNPs. All solution pH measurements were performed using a Sentron ISFET pH probe calibrated against aqueous standards.

Bioconjugation of CPNPs. To bioconjugate the CPNPs with avidin, a 1 mL aliquot of CPNPs in their 70% ethanol solution was first dried under argon and covered from light until all of the solvent evaporated and only the CPNPs remained. This dried sample was then reconstituted back to 1 mL with the addition of 1 mL of PBS (0.01 M phosphate buffer, 0.14 M NaCl, 0.01 M KCl at pH 7.4). This was then followed by the addition of 1 mL of 20 mg/mL 1-ethyl-3-[3-dimethylaminopropyl]carbodiimide hydrochloride (EDCI) (Sigma-Aldrich Co.) and 1 mL of 6 mg/mL avidin (Rockland Immunochemicals Inc.). Excess avidin was added in order to ensure the surface saturation of CPNPs. This reaction mix-

ture was incubated at 35 °C for 24 h in the dark with continuous stirring at 600 rpm.

After 24 h, the reaction mixture was centrifuge (Marathon 22K Centrifuge; Fischer Scientific Co.) filtered with a 100 kDa centrifuge filter device (Amicon Ultra-4, PLHK Ultracel-PL Membrane; Millipore Co.) to remove excess unconjugated avidin. Prior to use, the filtration membrane of the centrifuge filter device was washed with deionized H_2O in order to minimize nonspecific binding. A total of three centrifuge filtrations, each at 1000*g* for 30 min, were performed in order to maximize the removal of excess unconjugated avidin. After each centrifuge filtration step, the final volume of the retentate solution was brought back to the starting volume by the addition of PBS.

Multiple types of commercially available centrifuge filter devices, with different filtration membrane materials and chemistry, were evaluated to obtain minimal nonspecific adsorption and optimal washing of the CPNPs. The Millipore Amicon centrifuge filter device with 100 kDa nominal molecular weight limit Ultracel YM-100 regenerated cellulose membrane was identified as the product of choice. Centrifuge filter devices with a polyethersulfone filtration membrane were not feasible for this investigation due to significant nonspecific binding of the CPNPs to the filtration membrane.

The conjugation of biotinylated human holotransferrin or biotinylated anti-CD71 antibody to Avidin-CPNPs permits targeting of the transferrin receptor; the conjugation of biotinylated pentagastrin to Avidin-CPNPs permits targeting of the gastrin receptor. A 1 mL aliquot of 3.2 mg/mL biotin-conjugated human holotransferrin (Invitrogen Co.), 0.20 mL of 1 mg/mL biotin-conjugated anti-CD71 antibody (GeneTex Inc.), or 0.50 mL of 1 mg/mL biotin-conjugated pentagastrin (Bachem Co.) (in 0.1 N NH_4OH) was added to 1 mL of Avidin-CPNP complex. This reaction mixture was stirred at 600 rpm for 60 min at room temperature. The resulting Biomolecule-Avidin-CPNP complex was then filtered to remove excess unconjugated biomolecule (human holotransferrin, anti-CD71 antibody, or pentagastrin). Human Holotransferrin-Avidin-CPNPs and Anti-CD71-Avidin-CPNPs were filtered by tangential flow diafiltration using a 500 kDa molecular weight cutoff (MWCO) MicroKros hollow fiber tangential flow diafiltration device (Spectrum Laboratories Inc.). Pentagastrin-Avidin-CPNPs were centrifuge filtered with a 100 kDa centrifuge filter device (Amicon Ultra-4, PLHK Ultracel-PL Membrane; Millipore Co.). All of the Biomolecule-Avidin-CPNP samples were filtered three times in order to maximize the removal of excess unconjugated biomolecule. After each filtration step, the final volume of the retentate solution was brought back to the starting volume by the addition of PBS.

The conjugation of gastrin-10 to CPNPs *via* the PEG−maleimide coupling strategy permits targeting of the gastrin receptor as previously described by Sosabowski and colleagues.[35] A 9 mL aliquot of Citrate-CPNPs was chemically conjugated with maleimide polyethylene glycol amine (PEG−maleimide; JenKem Technology Inc.), through the ethyl-*N*-(3-dimethylaminopropyl)-*N*′-hydrochloride carbodiimide reaction (EDCI, Fluka BioChemika ≥99.0% (AT); Sigma-Aldrich Co.). The sample was first stirred at 550 rpm on a combined magnetic stir/hot plate set to 50 °C. In a dropwise manner, 1 mL of EDCI (1 mg/mL) followed by 1 mL of PEG−maleimide (10 mg/mL), both in aqueous solutions of CO_2-free deionized H_2O (pH 7), were added to the sample under continuous stirring, to produce a calculated 6-fold excess for monolayer surface coverage. The particles were allowed to react for 15 h at 50 °C to form amide linkages between the carboxylate surfaces and the PEG−maleimide. The mixture was then centrifuge filtered through a 100 kDa filter (Amicon Ultra-4, PLHK Ultracel-PL Membrane; Millipore Co.) at 5000*g* for 2 min to remove any excess EDCI and unreacted PEG−maleimide. The characterization of the resulting Maleimide-PEG-CPNPs in the retentate showed that the CPNPs remained well-dispersed after the centrifugation wash. The gastrin-10 peptide has a cysteine residue for covalent attachment. Thus, the gastrin-10 was added at a 5:1 molar excess to the Maleimide-PEG-CPNPs. This solution was incubated overnight at 4 °C, protected from light, to produce Gastrin-10-PEG-CPNPs.

Characterization of Nanoparticles. Particle size distributions for the CPNPs were obtained through dynamic light scattering (DLS) using a Malvern Nano-S Zetasizer. Transmission electron microscopy (TEM) was performed using a JEOL JEM 1200 EXII instrument on dried nanoparticles prepared on a carbon film grid with a copper backing. To verify that avidin was grafted on the CPNPs, ζ potential distributions were obtained using a Brookhaven ZetaPALS ζ potential analyzer. To quantify and test the bioactivity of avidin grafted on CPNPs, a fluorometric assay for avidin−biotin interaction based on the displacement of the fluorescent probe 2-anilinonaphthalene-6-sulfonic acid (2,6-ANS) was utilized.[22]

A 4.85 mg/mL solution of 2,6-ANS (Molecular Probes, Invitrogen Co.) was prepared in 1 mL of deionized H_2O. A 24 μg/mL solution of biotin was prepared in 10 mL of deionized H_2O to produce the biotin solution for the assay. The 2,6-ANS solution, followed by the biotin solution, was titrated in 0.50 μL aliquots into the Avidin-CPNP solution to obtain a sufficient number of data points. The reaction mixture was stirred for 1 min after the addition of each aliquot to the Avidin-CPNP solution to allow enough time for a homogeneous reaction mixture and to maintain consistency with respect to reaction time throughout the experiment. The fluorescence spectra were recorded with a PTI fluorometer in which emitted radiation is collected at 90° with a photomultiplier tube (PMT) detector. The sample is excited by a xenon arc lamp whose illumination passes through a 5 nm bandwidth slit and a monochromator to select the excitation wavelength. For the emission scan, the excitation wavelength was set to 328 nm and the emission wavelength range was set to 350−625 nm.

Cell Culture. Human MDA-MB-231 breast cancer cells were cultured in DMEM supplemented with 10% fetal bovine serum (FBS) and 1% antibiotic/antimycotic solution (Invitrogen, Carlsbad, CA). Human BxPC-3 pancreatic cancer cells were cultured in RPMI-1640 supplemented with 10% FBS and 1% antibiotic/antimycotic solution. All cell cultures were maintained at 37 °C and 5% CO_2. Cells were harvested by trypsin/EDTA detachment for subculture or tumor engraftment.

Fluorescence Microscopy. Cells were grown on coverslips under normal media conditions and then incubated with targeted or untargeted CPNPs followed by a media exchange. Cells were fixed in 2% (w/v) paraformaldehyde and mounted onto glass slides. Cells were visualized using a Nikon Eclipse E400 microscope through a 40× objective using a combination Nikon DAPI/FIT-C filter cube and recorded on a Nikon Coolpix 995 digital camera.

Flow Cytometry. Cells were detached from tissue culture-ware, surface Fc receptors blocked with appropriate IgG, incubated with specific antibodies (antihuman CD71-FITC or-PE, eBiosciences, San Diego, CA), and fixed in 2% (w/v) paraformaldehyde. Samples were analyzed on a BD Biosciences (San Jose, CA) LSR II Special Order flow cytometer in the Penn State College of Medicine Flow Cytometry Core, utilizing appropriate compensation controls. Data analysis was performed using BD Biosciences FACS Diva software.

***In Vivo* Tumor Xenograft.** All animal procedures were approved by the Pennsylvania State University Institutional Animal Care and Use Committee. Four to six week old female athymic nude mice were purchased from Harlan (Indianapolis, IN). Subcutaneous breast cancer xenografts were prepared as previously described.[2] Briefly, 1×10^7 MDA-MB-231 cells, prepared in 100 μL of growth media, were engrafted by subcutaneous injection. Orthotopic pancreatic cancer xenografts were prepared as previously described.[32] Briefly, mice were fully anesthetized with a mixture of ketamine-HCl (129 mg/kg) and xylazine (4 mg/kg) injected intramuscularly. A small incision was made in the left flank, the peritoneum was dissected, and the pancreas exposed. Using a 27 gauge needle, 1×10^6 BxPC-3 cells, prepared in 100 μL of Hank's balanced salt solution, were injected into the pancreas. All xenografted or orthotopic tumors were allowed to establish for 1 week prior to experimentation.

***In Vivo* Imaging.** CPNPs, or controls, were diluted 1:10 into sterile isotonic NaCl, and 100 μL was injected *via* tail vein into tumor-bearing mice. Equivalent ICG concentrations were determined prior to injection *via* absorption spectroscopy (2×10^{-6} M prior to dilution). Whole animal imaging was performed as previously described.[2] Briefly, anesthesia was induced and maintained by inhalation of 5% IsolSol (Vedco, St. Joseph, MO) in 100% oxygen. Near-infrared transillumination images (755 nm excitation, 830 nm emission, 3 min exposure) and corresponding X-ray images

were obtained with an *In Vivo* FX whole animal imaging station (Carestream Health, Rochester, NY). Signal distribution relative to anatomy was illustrated by merging near-infrared and X-ray images.

Acknowledgment. This work was funded, in part, by a grant from the Children's Miracle Network to B.M.B. to evaluate targeted nanotherapies and NIH Grant NIH R01 CA117926 to J.P.S. This work was also partially supported by Keystone Nano, Inc. J.H.A. and M.K. are CSO and CMO, respectively.

REFERENCES AND NOTES

1. Morgan, T. T.; Muddana, H. S.; Altiynoğlu, E. Ý; Rouse, S. M.; Tabakovicí, A.; Tabouillot, T.; Russin, T. J.; Shanmugavelandy, S. S.; Butler, P. J.; Eklund, P. C.; *et al.* Encapsulation of Organic Molecules in Calcium Phosphate Nanocomposite Particles for Intracellular Imaging and Drug Delivery. *Nano Lett.* **2008**, *8*, 4108–4115.
2. Altıynoğlu, E. İ.; Russin, T. J.; Kaiser, J. M.; Barth, B. M.; Eklund, P. C.; Kester, M.; Adair, J. H. Near-Infrared Emitting Fluorophore-Doped Calcium Phosphate Nanoparticles for *In Vivo* Imaging of Human Breast Cancer. *ACS Nano* **2008**, *2*, 2075–2084.
3. Kester, M.; Heakal, Y.; Fox, T.; Sharma, A.; Robertson, G. P.; Morgan, T. T.; Altıynoğlu, E. İ.; Tabaković, A.; Parette, M. R.; Rouse, S. M.; *et al.* Calcium Phosphate Nanocomposite Particles for *In Vitro* Imaging and Encapsulated Chemotherapeutic Drug Delivery to Cancer Cells. *Nano Lett.* **2008**, *12*, 4116–4121.
4. Muddana, H. S.; Morgan, T. T.; Adair, J. H.; Butler, P. J. Photophysics of Cy3-Encapsulated Calcium Phosphate Nanoparticles. *Nano Lett.* **2009**, *4*, 1559–1566.
5. Daniels, T. R.; Delgado, T.; Helguera, G.; Penichet, M. L. The Transferrin Receptor Part II: Targeted Delivery of Therapeutic Agents into Cancer Cells. *Clin. Immunol.* **2006**, *121*, 159–176.
6. Daniels, T. R.; Delgado, T.; Rodriguez, J. A.; Helguera, G.; Penichet, M. L. The Transferrin Receptor Part I: Biology and Targeting with Cytotoxic Antibodies for the Treatment of Cancer. *Clin. Immunol.* **2006**, *121*, 144–158.
7. Omary, M. B.; Trowbridge, I. S.; Minowada, J. Human Cell-Surface Glycoprotein with Unusual Properties. *Nature* **1980**, *286*, 888–891.
8. Shindelman, J. E.; Ortmeyer, A. E.; Sussman, H. H. Demonstration of the Transferrin Receptor in Human Breast Cancer Tissue. Potential Marker for Identifying Dividing Cells. *Int. J. Cancer* **1981**, *27*, 329–334.
9. Sutherland, R.; Delia, D.; Schneider, C.; Newman, R.; Kemshead, J.; Greaves, M. Ubiquitous Cell-Surface Glycoprotein on Tumor Cells Is Proliferation-Associated Receptor for Transferrin. *Proc. Natl. Acad. Sci. U.S.A.* **1981**, *78*, 4515–4519.
10. Gosk, S.; Vermehren, C.; Storm, G.; Moos, T. Targeting Anti-Transferrin Receptor Antibody (Ox26) and Ox26-Conjugated Liposomes to Brain Capillary Endothelial Cells Using *In Situ* Perfusion. *J. Cereb. Blood Flow Metab.* **2004**, *11*, 1193–1204.
11. Huwyler, J.; Drewe, J.; Krähenbuhl, S. Tumor Targeting Using Liposomal Antineoplastic Drugs. *Int. J. Nanomed.* **2008**, *3*, 21–29.
12. Smith, J. P.; Fantaskey, A.; Liu, G.; Zagon, I. S. Identification of Gastrin as a Growth Peptide in Human Pancreatic Cancer. *Am. J. Physiol.* **1995**, *268*, R135–R141.
13. Smith, J. P.; Stock, E. A.; Wotring, M. G.; McLaughlin, P. J.; Zagon, I. S. Characterization of the CCK-B/Gastrin-like Receptor in Human Colon Cancer. *Am. J. Physiol.* **1996**, *271*, R796–R805.
14. Wank, S. A.; Pisegna, J. R.; de Weerth, A. Brain and Gastrointestinal Cholecystokinin Receptor Family: Structure and Functional Expression. *Proc. Natl. Acad. Sci. U.S.A.* **1992**, *89*, 8691–8695.
15. Kopin, A. S.; Lee, Y. M.; McBride, E. W.; Miller, L. J.; Lu, M.; Lin, H. Y.; Kolakowski, L. F., Jr.; Beinborn, M. Expression Cloning and Characterization of the Canine Parietal Cell Gastrin Receptor. *Proc. Natl. Acad. Sci. U.S.A.* **1992**, *89*, 3605–3609.
16. Soll, A. H.; Berglindh, T. *Receptors That Regulate Gastric Acid-Secretory Function*, 3rd ed.; Raven Press: New York, 1994; Vol. 1, pp 1139−1170.
17. Johnson, L. R.; McCormack, S. A. *Regulation of Gastrointestinal Mucosal Growth*, 3rd ed.; Raven Press: New York, 1994; Vol. 1, pp 611−642.
18. Smith, J. P.; Shih, A. H.; Wotring, M. G.; McLaughlin, P. J.; Zagon, I. S. Characterization of CCK-B/Gastrin-like Receptors in Human Gastric Carcinoma. *Int. J. Oncol.* **1998**, *12*, 411–419.
19. Smith, J. P.; Liu, G.; Soundararajan, V.; McLaughlin, P. J.; Zagon, I. S. Identification and Characterization of CCK-B/Gastrin Receptors in Human Pancreatic Cancer Cell Lines. *Am. J. Physiol.* **1994**, *266*, R277–R283.
20. Smith, J. P.; Verderame, M. F.; McLaughlin, P.; Martenis, M.; Ballard, E.; Zagon, I. S. Characterization of the CCK-C (Cancer) Receptor in Human Pancreatic Cancer. *Int. J. Mol. Med.* **2002**, *10*, 689–694.
21. Jemal, A.; Siegel, R.; Ward, E.; Hao, Y.; Xu, J.; Murray, T.; Thun, M. J. Cancer Statistics. *CA Cancer J. Clin.* **2008**, *58*, 71–96.
22. Mock, D. M.; Langford, G.; Dubois, D.; Criscimagna, N.; Horowitz, P. A Fluorometric Assay for the Biotin−Avidin Interaction Based on Displacement of the Fluorescent Probe 2-Anilinonaphthalene-6-Sulfonic Acid. *Anal. Biochem.* **1985**, *151*, 178–181.
23. Livnah, O.; Bayer, E. A.; Wilchek, M.; Sussman, J. L. Three-Dimensional Structures of Avidin and the Avidin−Biotin Complex. *Proc. Natl. Acad. Sci. U.S.A.* **1993**, *90*, 5076–5080.
24. Morag, E.; Bayer, E. A.; Wilchek, M. Reversibility of Biotin-Binding by Selective Modification of Tyrosine in Avidin. *Biochem. J.* **1996**, *316*, 193–199.
25. Pardridge, W. M. Brain Drug Delivery and Blood-Brain Barrier Transport. *Drug Delivery* **1993**, *1*, 83–101.
26. Sjoback, R.; Nygren, J.; Kubista, M. Absorption and Fluorescence Properties of Fluorescein. *Spectrochim. Acta A* **1995**, *6*, L7–L21.
27. Lakowicz, J. R. *Principles of Fluorescence Spectroscopy*, 3rd ed.; Springer: Baltimore, MD, 2006.
28. Madhankumar, A. B.; Slagle-Webb, B.; Wang, X.; Yang, Q. X.; Antonetti, D. A.; Miller, P. A.; Sheehan, J. M.; Connor, J. R. Efficacy of Interleukin-13 Receptor-Targeted Liposomal Doxorubicin in the Intracranial Brain Tumor Model. *Mol. Cancer Ther.* **2009**, *8*, 648–654.
29. Smith, J. P.; Shih, A.; Wu, Y.; McLaughlin, P. J.; Zagon, I. S. Gastrin Regulates Growth of Human Pancreatic Cancer in a Tonic and Autocrine Fashion. *Am. J. Physiol.* **1996**, *270*, R1078–R1084.
30. Brand, S. J.; Fuller, P. J. Differential Gastrin Gene Expression in Rat Gastrointestinal Tract and Pancreas During Neonatal Development. *J. Biol. Chem.* **1988**, *263*, 5341–5347.
31. Rozengurt, E.; Walsh, J. H. Gastrin, Cck, Signaling, and Cancer. *Annu. Rev. Physiol.* **2001**, *63*, 49–76.
32. Matters, G. L.; Harms, J. F.; McGovern, C. O.; Jayakumar, C.; Crepin, K.; Smith, Z. P.; Nelson, M. C.; Stock, H.; Fenn, C. W.; Kaiser, J.; *et al.* Growth of Human Pancreatic Cancer Is Inhibited by Down-Regulation of Gastrin Gene Expression. *Pancreas* **2009**, *38*, e151–e161.
33. Smith, J. P.; Verderame, M. F.; Ballard, E. N.; Zagon, I. S. Functional Significance of Gastrin Gene Expression in Human Cancer Cells. *Regul. Pept.* **2004**, *117*, 167–173.
34. Grimm, D.; Streetz, K. L.; Jopling, C. L.; Storm, T. A.; Pandey, K.; Davis, C. R.; Marion, P.; Salazar, F.; Kay, M. A. Fatality in Mice Due to Oversaturation of Cellular MicroRNA/Short Hairpin RNA Pathways. *Nature* **2006**, *441*, 537–541.
35. Sosabowski, J.; Lee, M.; Dekker, B.; Simmons, B.; Singh, S.; Bereford, H.; Hagan, S.; McKenzie, A.; Mather, S.; Watson, S. Formulation Development and Manufacturing of a Gastrin/CCK-2 Targeting Peptide as an Intermediate Drug Product for Clinical Imaging Study. *Eur. J. Pharm. Sci.* **2007**, *31*, 102–111.